Atmos. Chem. Phys., 19, 5235–5249, 2019
https://doi.org/10.5194/acp-19-5235-2019

Atmospheric Chemistry and Physics
Open Access
EGU

Characterization of nighttime formation of particulate organic nitrates based on high-resolution aerosol mass spectrometry in an urban atmosphere in China

Kuangyou Yu[1,2], Qiao Zhu[1], Ke Du[2], and Xiao-Feng Huang[1]

[1]Key Laboratory for Urban Habitat Environmental Science and Technology, School of Environment and Energy, Peking University Shenzhen Graduate School, Shenzhen, 518055, China
[2]Department of Mechanical and Manufacturing Engineering, University of Calgary, Calgary, Canada

Correspondence: Xiao-Feng Huang (huangxf@pku.edu.cn)

Received: 23 September 2018 – Discussion started: 8 October 2018
Revised: 1 April 2019 – Accepted: 1 April 2019 – Published: 17 April 2019

Abstract. Organic nitrates are important atmospheric species that significantly affect the cycling of NO_x and ozone production. However, characterization of particulate organic nitrates and their sources in polluted atmosphere is a big challenge and has not been comprehensively studied in Asia. In this study, an aerodyne high-resolution time-of-flight aerosol mass spectrometer (HR-ToF-AMS) was deployed at an urban site in China from 2015 to 2016 to characterize particulate organic nitrates in total nitrates with a high time resolution. Based on the cross-validation of two different data processing methods, organic nitrates were effectively quantified to contribute a notable fraction of organic aerosol (OA), namely 9 %–21 % in spring, 11 %–25 % in summer, and 9 %–20 % in autumn, while contributing a very small fraction in winter. The good correlation between organic nitrates and fresh secondary organic aerosol (SOA) at night, as well as the diurnal trend of size distribution of organic nitrates, indicated a key role of nighttime local secondary formation of organic nitrates. Furthermore, theoretical calculations of nighttime SOA production of NO_3 reactions with volatile organic compounds (VOCs) measured during the spring campaign were performed, resulting in three biogenic VOCs (α-pinene, limonene, and camphene) and one anthropogenic VOC (styrene) identified as the possible key VOC precursors to particulate organic nitrates. The comparison with similar studies in the literature implied that nighttime particulate organic nitrate formation is highly relevant to NO_x levels. This study proposes that unlike the documented cases in the United States and Europe, modeling nighttime particulate organic nitrate formation in China should incorporate not only biogenic VOCs but also anthropogenic VOCs for urban air pollution, which needs the support of relevant smog chamber studies in the future.

1 Introduction

Organic nitrates (ONs) in aerosols have an important impact on the fate of NO_x and ozone production (Lelieveld et al., 2016), which can be formed in a minor channel of the reaction between peroxy radicals (RO_2) and NO (Reactions R1 and R2; usually, an increased fraction of this reaction leads to the formation of alkoxy radicals (RO) and NO_2 – Reaction R3) or via the NO_3-induced oxidation of unsaturated hydrocarbons (R=R′) (Reaction R4). Even though some recent studies have suggested that the formation of organic nitrates from peroxy radicals and NO may play a larger role than previously recognized (Teng et al., 2015, 2017), yields of organic nitrates via NO_3 reacting with alkenes are generally much higher (Fry et al., 2009; Ayres et al., 2015; Boyd et al., 2015, 2017):

$$RH + OH + O_2 \rightarrow RO_2 + H_2O, \quad (R1)$$

$$RO_2 + NO \rightarrow RONO_2, \quad (R2)$$

$$RO_2 + NO \rightarrow RO + NO_2 \quad (R3)$$

$$R = R' + NO_3 \rightarrow R(ONO_2)R'. \quad (R4)$$

Several methods have been developed to directly measure total organic nitrates (gas plus particle) in the real atmosphere. For example, Rollins et al. (2012) used a thermal-

dissociation laser-induced fluorescence technique (TD-LIF) to observe organic nitrates in the United States; Sobanski et al. (2017) measured organic nitrates in Germany using the thermal-dissociation cavity ring-down spectroscopy (TD-CRDS). Field and laboratory studies around the world indicated that particulate organic nitrates could contribute a large portion of secondary organic aerosol (SOA; Rollins et al., 2012; Xu et al., 2015a; Fry et al., 2013; Ayres et al., 2015; Boyd et al., 2015; Lee et al., 2016). Recently, researchers have proposed some estimation methods for particle-phase organic nitrates based on aerosol mass spectrometry (AMS) with a high time resolution (Farmer et al., 2010; Hao et al., 2014; Xu et al., 2015a, b). Ng et al. (2017) reviewed the nitrate radical chemistry and the abundance of particulate organic nitrates in the United States and Europe and further concluded that particulate organic nitrates are formed substantially via NO_3+BVOC chemistry, which plays an important role in SOA formation. Unfortunately, relevant Chinese datasets are still scarce and not included in this review. This was because (1) the contributions of organic nitrates in SOA and total nitrates in the Chinese atmosphere remain poorly understood and (2) the anthropogenic and biogenic precursor emissions in China are significantly different from those in the United States and Europe and thus cannot be easily estimated. To our best knowledge, few studies have investigated the concentrations and formation pathways of particulate organic nitrates in China. Xu et al. (2017) estimated the mass concentration of organic nitrogen in Beijing using AMS, but in this study, they ignored the contribution of NO_x^+ family, which are the major fragments of organic nitrates.

Shenzhen is a megacity of China in a subtropical region, where NO_x-involved photochemical reactions are very active, given considerable biogenic and anthropogenic volatile organic carbon (VOC) emissions (Zhang et al., 2008). To assess the evolution of particulate organic nitrates in a polluted urban atmosphere, we deployed an aerodyne high-resolution time-of-flight aerosol mass spectrometer (HR-ToF-AMS) and other instruments in Shenzhen from 2015 to 2016 in this study. Organic nitrates and their contributions to organic aerosol (OA) in different seasons were estimated by different methods using the HR-ToF-AMS datasets based on which the secondary formation pathway of particulate organic nitrates in Shenzhen was further explored.

2 Experiment methods

2.1 Sampling site and period

The sampling site (22.6° N, 113.9° E) was on the roof (20 m above ground) of an academic building on the campus of the Peking University Shenzhen Graduate School (PKUSZ), which is located in the western urban area in Shenzhen (Fig. 1). This site is mostly surrounded by subtropical plants without significant anthropogenic emission sources nearby, except for a local road that is ∼ 100 m from the site. In this study, we used the statistical data from the Meteorological Bureau of Shenzhen Municipality (http://weather.sz.gov.cn/, last access: 10 March 2019) as the reference data to determine the sampling periods for four different seasons during 2015–2016, as shown in Table 1.

2.2 Instrumentation

2.2.1 High-resolution time-of-flight aerosol mass spectrometer

During the sampling periods, chemical composition of non-refractory PM_1 was measured by an aerodyne HR-ToF-AMS, and detailed descriptions of this instrument are given in the literature (DeCarlo et al., 2006; Canagaratna et al., 2007). The setup and operation of the HR-ToF-AMS can be found in our previous publications (Huang et al., 2010, 2012; Zhu et al., 2016). To remove coarse particles, a $PM_{2.5}$ cyclone inlet was installed before the sampling copper tube with a flow rate of 10 L min^{-1}. Before entering the AMS, the sampled air was dried by a Nafion dryer (MD-070-12S-4, Perma Pure Inc.) to eliminate the potential influence of relative humidity on particle collection (Matthew et al., 2008). The ionization efficiency (IE) calibrations were performed using pure ammonium nitrate every 2 weeks. The relative ionization efficiencies (RIEs) used in this study were 1.2 for sulfate, 1.1 for nitrate, 1.3 for chloride, 1.4 for organics, and 4.0 for ammonium (Jimenez et al., 2003). Composition-dependent collection efficiencies (CEs) were applied to the data according to the method in Middlebrook et al. (2012). The instrument was operated at two ion optical modes with a cycle of 4 min, including 2 min for the mass-sensitive V mode and 2 min for the high-mass-resolution W mode. The HR-ToF-AMS data analysis was performed using the software SQUIRREL (version 1.57) and PIKA (version 1.16) written in Igor Pro 6.37 (WaveMetrics Inc.; http://cires1.colorado.edu/jimenez-group/ToFAMSResources/ToFSoftware/index.html, last access: 10 March 2019).

2.2.2 Other co-located instruments

In addition to the HR-ToF-AMS, other relevant instruments were deployed at the same sampling site. An aethalometer (AE-31, Magee) was used for measurement of refractory black carbon (BC) with a resolution of 5 min. A scanning mobility particle sizer (SMPS) system (3775 CPC and 3080 DMA, TSI Inc.) was used to obtain the particle number size distribution in 15–615 nm (mobility diameter) with a time resolution of 5 min. Ozone and NO_x were measured by a 49i ozone analyzer and a 42i nitrogen oxide analyzer (Thermo Fisher Scientific), respectively. In the spring campaign, ambient VOC concentrations were also measured using an online VOC monitoring system (TH-300B, Tianhong

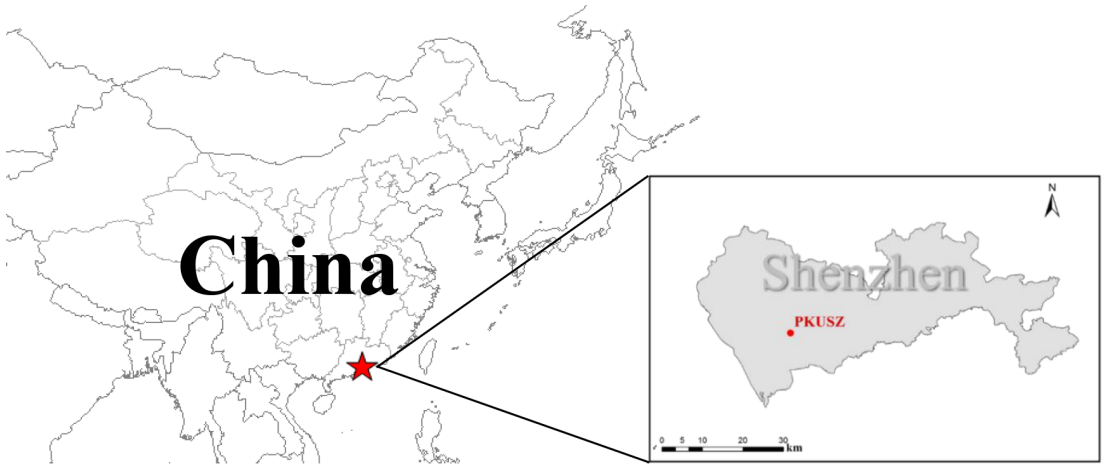

Figure 1. The location of the sampling site.

Table 1. Meteorological conditions, PM_1 species concentrations, and relevant parameters for different sampling periods in Shenzhen.

Sampling period		4.1–4.30, 2016 spring	8.1–8.31, 2015 summer	11.4–11.30, 2015 autumn	1.21–2.3, 2016 winter
Meteorology	T (°C)	24.5 ± 2.5	29.0 ± 3.0	23.6 ± 3.7	10.7 ± 4.7
	RH (%)	78.0 ± 12.7	71.2 ± 17.5	68.2 ± 15.8	75.4 ± 18.7
	Wind speed (WS) ($m\,s^{-1}$)	1.4 ± 0.8	1.0 ± 0.7	1.2 ± 0.7	1.5 ± 0.8
Species ($\mu g\,m^{-3}$)	Organics	4.3 ± 3.2	10.0 ± 6.9	7.8 ± 5.9	5.1 ± 3.5
	SO_4^{2-}	3.2 ± 1.8	5.8 ± 3.3	2.3 ± 1.5	1.9 ± 1.2
	Total NO_3^-	0.96 ± 1.4	0.91 ± 0.90	1.3 ± 1.4	1.6 ± 1.0
	NH_4^+	1.4 ± 0.8	2.0 ± 1.1	1.1 ± 0.8	1.2 ± 0.6
	Cl^-	0.14 ± 0.19	0.03 ± 0.05	0.22 ± 0.36	0.64 ± 0.85
	BC	1.9 ± 2.1	2.4 ± 1.6	3.5 ± 2.6	2.4 ± 1.5
	Total	12.0 ± 8.9	15.1 ± 13.8	11.8 ± 9.5	12.2 ± 7.2
ON-relevant parameters	$R_{NH_4NO_3}$	2.80	3.20	3.32	3.48
	R_{obs}	3.74	6.14	4.30	3.55
	Fraction of positive numbers of $R_{obs}-R_{NH_4NO_3}$	99 %	99 %	84 %	47 %

Corp.), including an ultralow-temperature preconcentration cold trap and an automated in situ gas chromatograph (Agilent 7820A) equipped with a mass spectrometer (Agilent 5977E). The system had both a flame ionization detector (FID) gas channel for C2–C5 hydrocarbons and a mass spectrometer (MS) gas channel for C5–C12 hydrocarbons, halohydrocarbons, and oxygenated VOCs. A complete working cycle of the system was 1 h and included six steps: sample collection, freeze trapping, thermal desorption, gas chromatography with flame ionization detector–mass spectrometer (GC-FID/MS) analysis, heating, and anti-blowing purification. The sample collection time was 5 min. The sampling flow speed was $60\,mL\,min^{-1}$. The anti-blowing flow speed was $200\,mL\,min^{-1}$. The calibration of over 100 VOCs was performed using mixed standard gas before and after the campaign. Detection limits for most compounds were near 5 pptv. A more detailed description of this instrument can be found in Wang et al. (2014).

2.3 Organic nitrate estimation methods

In this study, we used two independent methods to estimate particulate organic nitrates based on the AMS data, following the approaches in Xu et al. (2015b). The first method is based on the NO^+/NO_2^+ ratio (NO_x^+ ratio) in the HR-ToF-AMS. Due to the very different NO_x^+ ratios of organic nitrates and inorganic nitrate (i.e., R_{ON} and $R_{NH_4NO_3}$, respectively; Farmer et al., 2010; Boyd et al., 2015; Fry et al., 2009; Bruns et al., 2010), the NO_2^+ and NO^+ concentrations of organic nitrates ($NO_{2,ON}$ and NO_{ON}) can be quantified with the HR-ToF-AMS data via Eqs. (1) and (2), respectively (Farmer

et al., 2010):

$$NO^+_{2,ON} = \frac{NO^+_{2,obs} \times (R_{obs} - R_{NH_4NO_3})}{R_{ON} - R_{NH_4NO_3}}, \quad (1)$$

$$NO^+_{ON} = R_{ON} \times NO_{2,ON}, \quad (2)$$

where R_{obs} is the NO^+_x ratio from the observation. The value of R_{ON} is difficult to determine because it varies between instruments and precursor VOCs. However, $R_{NH_4NO_3}$ was determined by IE calibration using pure NH_4NO_3 every 2 weeks for each campaign, and the results showed stable values. In spring, the average $R_{NH_4NO_3}$ was 2.66 for the first IE calibration and 2.94 for the second one. In summer, the average $R_{NH_4NO_3}$ was 3.05 and 3.34 for the first and second IE calibrations, respectively. In autumn, the average $R_{NH_4NO_3}$ was 3.33 and 3.31 for the first and second IE calibrations, respectively. In winter, the average $R_{NH_4NO_3}$ was 3.45 and 3.51 for the first and second IE calibrations, respectively. We adopted the $R_{ON}/R_{NH_4NO_3}$ estimation range (from 2.08 to 3.99) for variation in precursor VOCs in the literature to determine R_{ON} (Farmer et al., 2010; Boyd et al., 2015; Bruns et al., 2010; Sato et al., 2010; Xu et al., 2015b), and thus two R_{ON} values were calculated for each season to provide the upper bound ($NO_{3\_org\_ratio\_1}$) and lower bound ($NO_{3\_org\_ratio\_2}$) of $NO_{3,org}$ mass concentration.

The second method is based on the traditional positive matrix factorization (PMF) analysis of HR organic mass spectra, which resolves different organic factors (Zhang et al., 2011; Ng et al., 2010; Huang et al., 2013). Combined with NO^+ and NO^+_2 ions, the same analysis of HR organic mass spectra was performed to separate NO^+ and NO^+_2 ions into different organic factors and an inorganic nitrate factor (Hao et al., 2014; Xu et al., 2015b). The PMF analysis procedures in this study can be found in our previous publications (Huang et al., 2010; Zhu et al., 2016; He et al., 2011), resulting in three organic factors and one inorganic factor in spring, summer, and autumn: a hydrocarbon-like OA (HOA) characterized by $C_nH^+_{2n+1}$ and $C_nH^+_{2n-1}$ and O/C values of 0.11 to 0.18; a less-oxidized oxygenated OA (LO-OOA) characterized by $C_xH_yO^+_z$, especially $C_2H_3O^+$ and O/C values of 0.28 to 0.70; a more-oxidized oxygenated OA (MO-OOA) also characterized by $C_xH_yO^+_z$, especially CO^+_2 and O/C values of 0.78 to 1.24; and a nitrate inorganic aerosol (NIA) characterized by overwhelming NO^+ and NO^+_2 values, as indicated in Fig. S6 in the Supplement. According to the diagnostic plots of the PMF analysis shown in Figs. S2 to S4, the same organic factors as those in the traditional PMF analysis of only organic mass spectra were obtained. The NO^+ and NO^+_2 ions were distributed among different OA factors and the NIA factor; thus the concentrations of nitrate functionality (NO^+_{org} and $NO^+_{2,org}$) in organic nitrates ($NO_{3,org}$) are equal to the sum of NO^+_2 and NO^+ via Eqs. (3) and (4), respectively (Xu et al., 2015b):

$$NO^+_{2,org} = \sum([\text{OA factor}]_i \times f_{NO_2,i}), \quad (3)$$

$$NO^+_{org} = \sum([\text{OA factor}]_i \times f_{NO,i}), \quad (4)$$

where $[\text{OA factor}]_i$ represents the mass concentration of OA factor i, and $f_{NO_2,i}$ and $f_{NO,i}$ represent the mass fractions of NO^+_2 and NO^+, respectively.

It should be noted that the four-factor solution seemed to have a "mixed factor" problem to some extent (Zhu et al., 2018). For example, HOA mixed with cooking OA (COA; clear $C_3H_3O^+$ in m/z 55 for spring, summer, and autumn; Mohr et al., 2012), and biomass burning OA (BBOA) mixed with LO-OOA (clear m/z 60 and 73 signals in LO-OOA in autumn; Cubison et al., 2011). However, running PMF with more factors would produce unexplained factors but less influence on the apportionment of NO^+ and NO^+_2 ions between organic nitrates and inorganic nitrate (Table S1 in the Supplement). In addition, the standard deviations of NO^+ and NO^+_2 ions in the OA factors across different rotational forcing parameter (Fpeak) values (from −1.0 to 1.0) were very small (Table S2). Therefore, the four-factor solution was used for quantifying organic nitrates in spring, summer, and autumn.

3 Results and discussion

3.1 Organic nitrate estimation

Table 2 shows the concentrations of nitrate functionality in organic nitrates (i.e., $NO_{3,org}$), estimated by both the NO^+/NO^+_2 ratio method and PMF method, as well as their contributions to the total measured nitrate. It should be noted that the small difference between the average R_{obs} and $R_{NH_4NO_3}$ in winter leads to a large portion of negative data using the NO^+/NO^+_2 ratio method (Table 1). The result from the PMF method shows that the contribution of organic nitrates to total nitrates is only 4.2 % in winter (Fig. S6), suggesting a negligible contribution of organic nitrates. Thus, we will only discuss organic nitrate estimation results in spring, summer, and autumn. The analytical outcomes by the NO^+/NO^+_2 ratio method and by the PMF method consistently suggest that organic nitrates had the highest ambient concentration (0.34–0.53 $\mu g\,m^{-3}$) and proportion in total nitrates (41 %–64 %) in summer compared to the different seasons. This finding agrees with the finding in Ng et al. (2017), and it implies a seasonal trend in comparison with that of total nitrates in Table 1. Assuming the average molecular weight of organic nitrates of 200 to 300 $g\,mol^{-1}$ (Rollins et al., 2012), we found that organic nitrates contributed 9 %–21 % to OA in spring, 11 %–25 % in summer, and 9 %–20 % in autumn.

In the PMF method, the mass fractions of organic nitrates in HOA, LO-OOA, and MO-OOA were 31 %, 49 %, and 20 %, respectively, in spring; 28 %, 52 %, and 20 %, respectively, in summer; and 30 %, 46 %, and 24 %, respectively, in

autumn. The major fraction of organic nitrates occurring in LO-OOA for the three seasons implied that organic nitrates were mostly related to fresher secondary OA formation. The NIA factors in all seasons were dominated by, but are not limited to, NO^+ and NO_2^+. Some organic fragments, such as CO_2^+ and $C_2H_3O^+$, are also part of these factors, which agreed with the findings in the literature (Hao et al., 2014; Xu et al., 2015b; Sun et al., 2012). This indicated the potential interference of organics in the NIA factor. It is also worth noting that the NO^+/NO_2^+ ratios in NIA (2.93 for spring, 3.53 for summer, and 3.54 for autumn) were higher than that for pure NH_4NO_3 (Table 1), indicating an underestimation of $NO_{3,org}$ concentration by the PMF method. This finding may also explain the reason that the concentration of $NO_{3,org}$ estimated using the PMF method was always close to the lower estimation bound of $NO_{3,org}$ concentration estimated using the NO^+/NO_2^+ ratio method in each season (Table 2).

To further verify the reliability of the estimated results of organic nitrates, the $NO_{3,org}$ concentration time series calculated by the two methods in each season are shown in Fig. 2a. The computed correlation coefficients (R) are good (0.82 for spring, 0.82 for summer, and 0.77 for autumn), indicating that similar results were achieved. The inorganic nitrate (NO_{3_inorg*}) obtained by subtracting $NO_{3\_org\_ratio\_1}$ from total measured nitrates also correlated well with the inorganic nitrate estimated using the PMF method ($R = 0.92$ for spring, 0.87 for summer, and 0.86 for autumn). While they were distinctive from those of inorganic nitrate (Fig. 2b), which indicates that organic nitrates had been separated well from inorganic nitrate in this study, the diurnal trends of organic nitrates obtained by the two methods were similar in each season, with lower concentrations in the daytime and higher concentrations at night.

3.2 Correlation between organic nitrates and OA factors

As indicated by the results in the PMF method, the majority of organic nitrates were associated with LO-OOA in spring, summer, and autumn in the urban atmosphere in Shenzhen, implying a dominant secondary origin of organic nitrates. To further confirm this relationship, we made the correlation analysis between organic nitrates estimated by the NO^+/NO_2^+ ratio method and the three factors resolved by the PMF analysis with only organic mass spectra in the three seasons. Generally, organic nitrates were found to correlate better with LO-OOA ($R = 0.69$–0.77 in Fig. 3) than with HOA and MO-OOA ($R = 0.03$–0.69 in Figs. S6–S8), which is consistent with the fact that the majority of organic nitrates were associated with LO-OOA in the PMF method. However, the moderate correlation between organic nitrates and HOA implied the possibility of direct emissions of organic nitrates. Furthermore, we found a noticeably improved correlation between LO-OOA and organic nitrates at night (19:00–06:00 LT) and a reduced correlation during the daytime (07:00–18:00 LT) in Fig. 3, especially in summer, implying that organic nitrate formation might be more closely related to secondary formation at night.

3.3 Size distribution characteristics of organic nitrates

In this section, we attempt to use the NO^+/NO_2^+ ratio as an indicator to investigate the size distribution characteristics of organic nitrates. Unfortunately, due to the lack of HR-PToF data, our analyses used the unit-mass resolution (UMR) PToF data of m/z 30 and 46, which might contain the interferences of $CH_2O_x^+$ (Fry et al., 2018). In our case, the time variations in contributions of CH_2O^+ in m/z 30 and $CH_2O_2^+$ in m/z 46 in the HR data of PM_1 for the four seasons are shown in Fig. S10. For all the four seasons, the average contributions of $CH_2O_x^+$ to m/z 30 and 46 in the HR data of PM_1 were less than 10 %, suggesting that the $m/z\,30$ / $m/z\,46$ ratio could mostly represent the NO^+/NO_2^+ ratio. The average size distributions of $m/z\,30$ and $m/z\,46$ for the four seasons are shown in Fig. S11, and Fig. 4a shows the average size distributions of different aerosol species and the $m/z\,30$ / $m/z\,46$ ratio in the four seasons. It is clearly found that the $m/z\,30$ / $m/z\,46$ ratio exhibited a decreasing trend in spring, summer, and autumn, while it remained constant in winter, similar to the value of $R_{NH_4NO_3}$ (red dotted line in Fig. 4a). In addition, in spring, summer, and autumn, the lowest values of the $m/z\,30$ / $m/z\,46$ ratio, occurring at $\sim 1\,\mu m$, were approximate to the corresponding seasonal values of $R_{NH_4NO_3}$. It should be noted that the similar size distribution patterns of the $m/z\,30$ / $m/z\,46$ ratio under the highest interferences (> 15 %) and lowest interferences (< 5 %) of $CH_2O_x^+$, indicated by the HR data of PM_1, for spring, summer, and autumn (Fig. S12) imply that the size distribution patterns of the $m/z\,30$ / $m/z\,46$ ratio were not affected significantly by the interferences of $CH_2O_x^+$. We also used the size distributions of the $m/z\,30$ / $m/z\,46$ ratio to separate the size distributions of inorganic and organic nitrates, as shown in Fig. S13, and the results indicate that organic nitrates were relatively more concentrated at small sizes compared to inorganic nitrates. Furthermore, the diurnal trends of the size distribution of the $m/z\,30$ / $m/z\,46$ ratio in spring, summer, and autumn in Fig. 4b show apparent higher values at small sizes at night, suggesting an important nighttime local origin of organic nitrates. Combining with the analysis in Sect. 3.2, the local nighttime secondary formation of organic nitrates in warmer seasons in the urban polluted atmosphere in Shenzhen is highlighted. This is consistent with the previous findings in the US and Europe that the nighttime NO_3+VOCs reactions serve as an important source for particulate organic nitrates (Rollins et al., 2012; Xu et al., 2015a, b; Fry et al., 2013; Lee et al., 2016). We will then explore the nighttime NO_3+VOCs reactions in Shenzhen in more detail in the following section.

Table 2. Summary of organic nitrate estimations using the NO^+/NO_2^+ ratio method and the PMF method.

Sampling period	NO^+/NO_2^+ ratio method				PMF method	
	$NO_{3,org}$ ($\mu g\,m^{-3}$)[a]		$NO_{3,org}/NO_3$		$NO_{3,org}$ ($\mu g\,m^{-3}$)[b]	$NO_{3,org}/NO_3$
	Lower	Upper	Lower	Upper		
Spring	0.12	0.19	13 %	21 %	0.12	12 %
Summer	0.34	0.53	41 %	64 %	0.39	43 %
Autumn	0.21	0.33	16 %	25 %	0.21	16 %
Winter	–	–	–	–	0.07	4.2 %

[a] $NO_{3,org}$ for upper bound is denoted as $NO_{3\_org\_ratio\_1}$, and $NO_{3,org}$ for lower bound is denoted as $NO_{3\_org\_ratio\_2}$. [b] $NO_{3,org}$ estimated using the PMF method is denoted as $NO_{3\_org\_PMF}$.

3.4 Nighttime particulate organic nitrate formation via NO_3+VOCs

Since online VOC measurement was only performed during the spring campaign (described in Sect. 2.2), the following theoretical analysis of NO_3+VOCs reactions applies only to the spring case. NO_3+VOCs reactions would yield a large mass of gas- and particle-phase organic nitrates (Rollins et al., 2012; Nah et al., 2016; Boyd et al., 2015, 2017; Xu et al., 2015a, b; Lee et al., 2016). We used Eq. (9) to roughly judge the production potential (PP) of organic nitrates from a NO_3+VOC reaction:

$$[\text{Production Potential}]_{NO_3+VOC_i} = K_i \cdot [VOC_i] \cdot [NO_3] \ , \quad (5)$$

where K_i represents the reaction rate coefficient for the NO_3 radical and a VOC. $[VOC_i]$ is the concentration of the specific VOC; $[NO_3]$ is the concentration of NO_3 radical. It should be noted that no organic nitrate yield parameter was introduced in Eq. (9) because only a few organic nitrate yields for biogenic VOCs (BVOCs) were available in the literature (Fry et al., 2014; Ng et al., 2017). However, given the fact that the values of $K_i \cdot [VOC_i] \cdot [NO_3]$ for different VOC species can differ by orders of magnitude, not multiplying the organic nitrate yields (ranging from 0 to 1) would not significantly affect the PP ranking of VOCs. In the spring campaign, the diurnal variations in NO_2, O_3, and estimated NO_3 radical concentrations are shown in Fig. S14. It was found that in comparison to the nighttime NO_3 radical concentration reported in literature in the United States (Rollins et al., 2012; Xu et al., 2015a), high concentration of NO_2 (19.93 ± 2.31 ppb) at night led to high yield of the NO_3 radical (1.24 ± 0.76 ppt) in Shenzhen, as calculated in Sect. S1 in the Supplement.

The reaction rate coefficients of typical measured nighttime VOC concentrations with the NO_3 radical and the production potentials are listed in Table S3 and shown in Fig. 5. These VOCs were considered based on their higher ambient concentrations and availability for reaction kinetics with NO_3 radical. According to the distribution of production potential, five BVOCs (i.e., α-pinene, limonene, camphene, β-pinene, and isoprene) and one anthropogenic VOC (styrene) were identified as notable VOC precursors with high production potential, while the sum of production potential from the other VOCs was negligible, as shown in Fig. 5b.

Based on the production potential evaluation above, we further explore SOA yield of NO_3 plus the six notable VOC precursors according to the analysis method of particulate organic nitrate formation in Xu et al. (2015a). Briefly, NO_3 and ozone are two main oxidants for SOA formation from VOCs at night. Based on the concentrations of oxidants and the reaction rate constants for VOCs with NO_3 and ozone, the branching ratio of each VOC that reacts with NO_3 can be estimated as in Eq. (10). By combining the estimated branching ratios and SOA yields from chamber studies (Table 3; where the chamber conditions to obtain the yields covered the range of aerosol mass loading in the spring campaign), potential SOA production from these VOCs can be calculated as in Eq. (11) (Xu et al., 2015a):

$$\text{branching ratio}_{\text{species } i+NO_3} = \frac{k_{[\text{species } i+NO_3]} \times [NO_3]}{k_{[\text{species } i+NO_3]} \times [NO_3] + k_{[\text{species } i+O_3]} \times [O_3]} \quad (6)$$

$$[SOA]_{\text{species,oxidant}} = [\text{species}] \times \text{branching ratio}_{\text{species,oxidant}} \times \text{yield}_{\text{species,oxidant}}. \quad (7)$$

The results in Table 3 show that all six notable VOC species were prone to react to NO_3 radical instead of O_3 at night, and the estimated potential SOA production from NO_3+VOCs reactions using SOA mass yields in the literature was 0–$0.33\,\mu g\,m^{-3}$ for α-pinene, 0.09–$1.28\,\mu g\,m^{-3}$ for limonene, $0.24\,\mu g\,m^{-3}$ for styrene, 0.004–$0.06\,\mu g\,m^{-3}$ for β-pinene, and 0.002–$0.02\,\mu g\,m^{-3}$ for isoprene. The SOA yield from camphene is currently unknown in the literature. It is seen that the average observed nighttime concentration of particulate organic nitrates during the spring campaign (0.39–$0.83\,\mu g\,m^{-3}$; converting NO_{3,org_ratio_1} and NO_{3,org_PMF} in Fig. 6 into organic nitrates assuming the average molecular weight of organic nitrates to be 200 to $300\,g\,mol^{-1}$) was well within the estimated SOA concentration ranges produced by α-pinene, limonene, and styrene in Table 3, indicating that

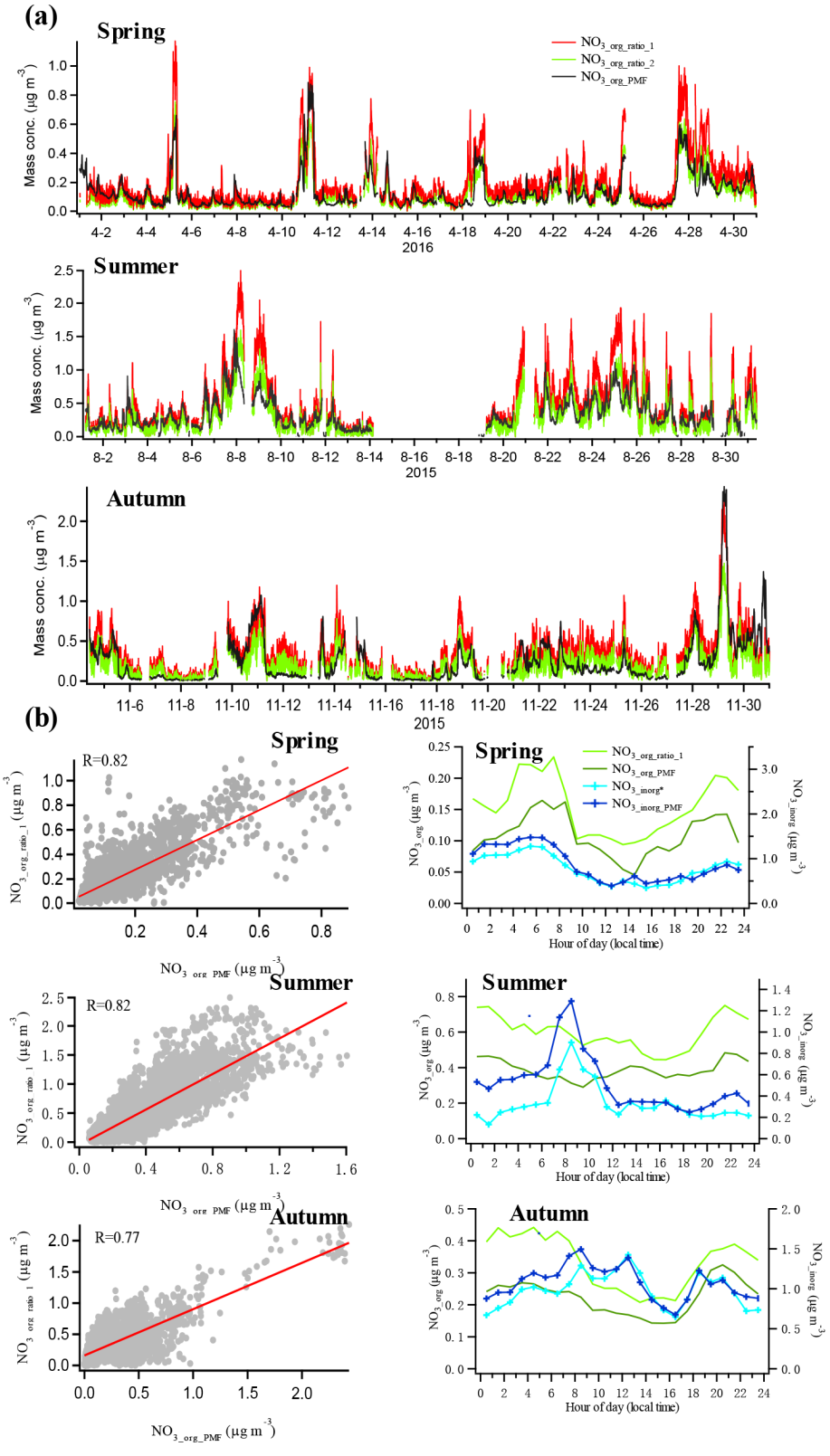

Figure 2. **(a)** Time series of $NO_{3,org}$ concentration estimated by the NO^+/NO_2^+ ratio method and PMF method for each season. **(b)** Correlations between $NO_{3\_org\_ratio\_1}$ and $NO_{3\_org\_PMF}$ (left panels); diurnal trends of organic nitrates and $NO_{3,org}$ estimated by the different methods (right panels).

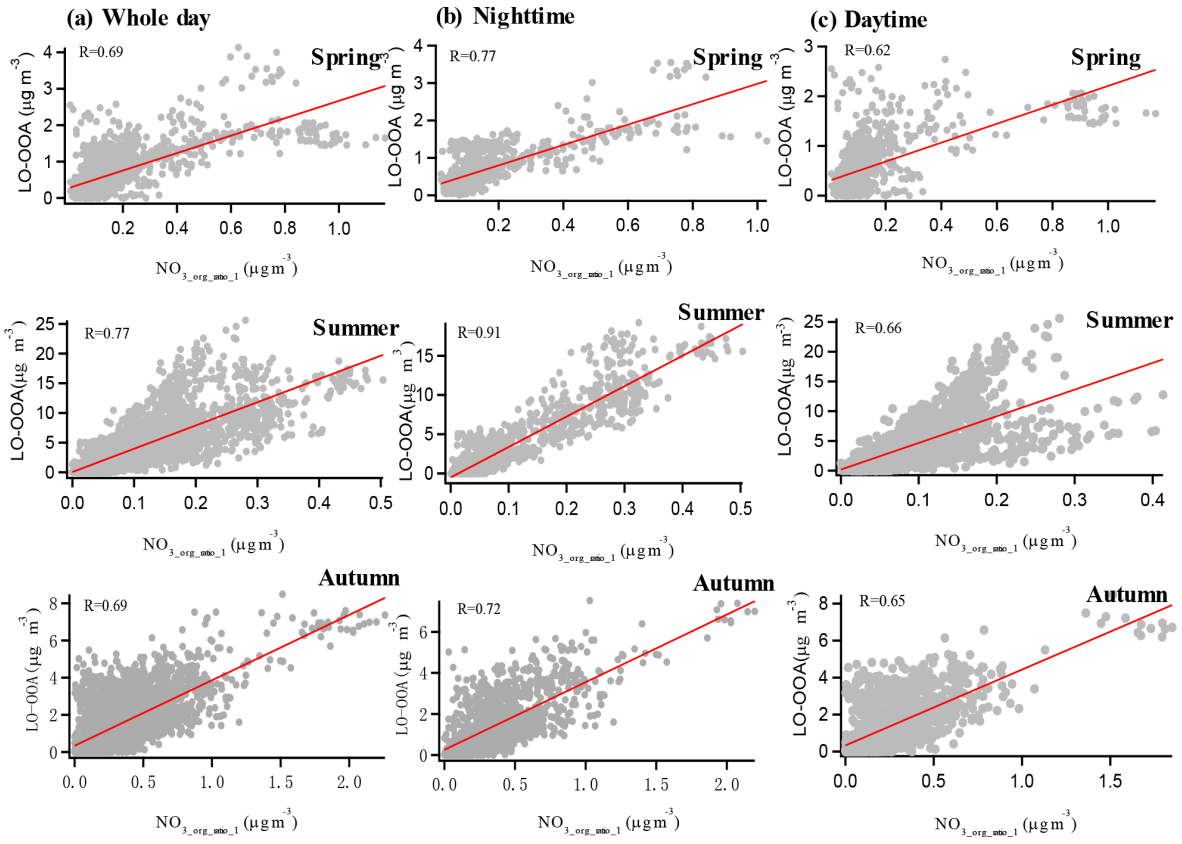

Figure 3. Correlation of $NO_{3\_org\_ratio\_1}$ and LO-OOA in each season for the whole day **(a)**, at night **(b)**, and in the daytime **(c)**.

these three VOCs were the key VOC precursors in the urban atmosphere in Shenzhen. Considering both the production potentials and SOA yields, the contributions of β-pinene and isoprene to nighttime formation of particulate organic nitrates could be negligible.

The estimation of potential SOA production above suggests significant contributions of α-pinene, limonene, and styrene to SOA, and the significant contribution of camphene is also possible. Thus, we further explore the diurnal variations in the PPs of these four VOCs. Figure 6 shows the diurnal trends of BC, LO-OOA, NO_{3,org_ratio_1}, NO_{3,org_PMF}, and the PPs of the four VOCs during the spring campaign. There were two apparent nighttime growth periods (i.e., I: 19:00–22:00 LT, II: 02:00–06:00 LT) for both NO_{3,org_ratio_1} and NO_{3,org_PMF}. During Period I, BC maintained a relatively higher level, suggesting stable anthropogenic emissions. In contrast, the increases in all the PPs during Period I indicated that these precursors contributed to the organic nitrate growth. After 22:00 LT, while the PPs still showed a rapid growth, BC and organic nitrates began to decrease, implying possible existence of other important anthropogenic VOC precursors, which were not identified by the GC-FID/MS analysis but would dominate the formation of organic nitrates at this stage. During Period II, the anthropogenic emissions remained at a stable lower level, as indicated by BC, while all the PPs increased with organic nitrates again, indicating that these four precursors also contributed to, or could dominate, this organic nitrate growth. As shown in Fig. S15, organic nitrates correlated better with the PPs ($R = 0.63$–0.74) than with LO-OOA ($R = 0.19$–0.31) or BC ($R = 0.02$–0.05) during Period II at the spring campaign, suggesting the significant contributions of the NO_3 reactions with these precursors.

It should be noted that all previous studies on nighttime organic nitrate formation in the US and Europe focused on mechanisms of NO_3 reactions with BVOCs (Hallquist et al., 1999; Spittler et al., 2006; Perraud et al., 2010; Fry et al., 2014; Nah et al., 2016; Boyd et al., 2015, 2017). In this study, however, we found that anthropogenic VOCs could also play significant roles in particulate organic nitrate formation at night. Besides styrene, one of the major aromatics (Cabrera-Perez et al., 2016), there were also other important anthropogenic VOC precursors that we did not identify in the spring campaign. In China, styrene has been actually identified as an important VOC of non-methane hydrocarbons (NMHCs) in urban areas and has a notable contribution to ozone formation and SOA production (An et al., 2009; Yuan et al., 2013; Zhu et al., 2019). This study highlights the possible key roles of anthropogenic VOC precursors in nighttime particulate organic nitrate formation in the urban

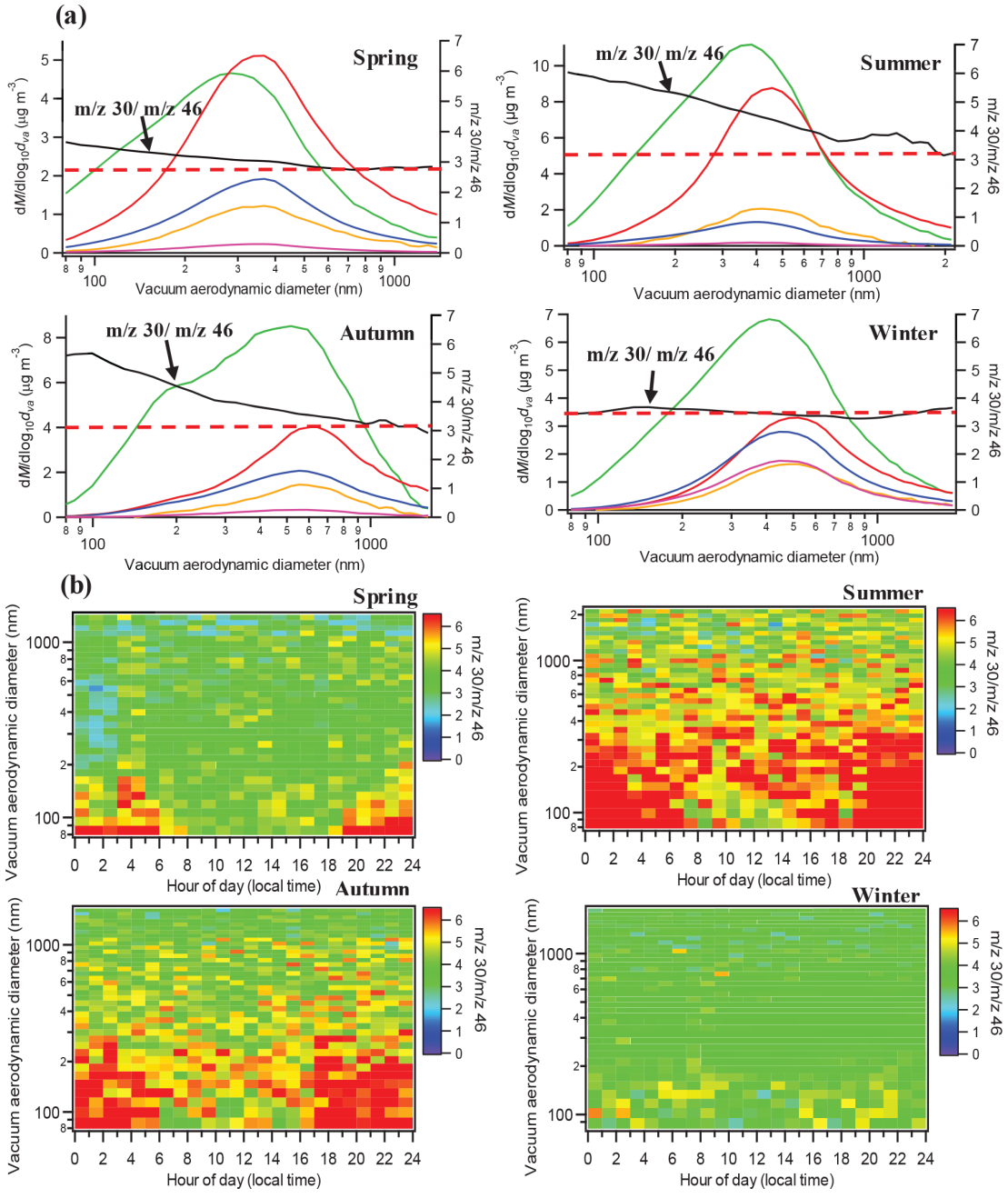

Figure 4. **(a)** Average size distributions of aerosol species and $m/z\,30$ / $m/z\,46$ ratio (red dotted line represents $R_{NH_4NO_3}$); **(b)** diurnal trends of size distribution of $m/z\,30$ / $m/z\,46$ ratio.

atmosphere in China, and relevant smog chamber studies for anthropogenic VOCs+NO_3 reactions are needed to support parameterization in modeling.

3.5 Comparison with other similar studies and implications

Table 4 shows the average ambient temperatures, average concentrations of NO, NO_2, monoterpenes, and $NO_{3,org}$; the ratio of $NO_{3,org}$ to $NO_{3,total}$; and the ratio of organic nitrates to total organics in several similar field campaigns available in the literature, which implies the key role of NO_3+VOCs reactions in nighttime particulate organic nitrate formation. In general, the variation in the particulate organic nitrate concentration is within an order of magnitude (0.06–0.98 μg m^{-3}) among the different sites. Higher concentrations of particulate organic nitrates generally are associated with higher NO_x concentrations rather than BVOC

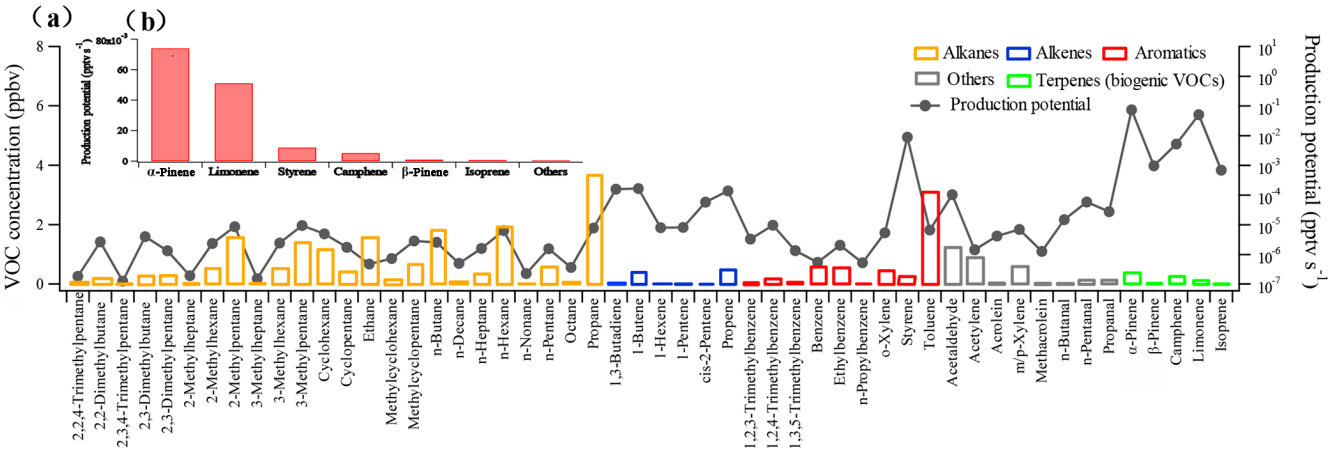

Figure 5. **(a)** Mean concentrations of VOCs and the corresponding calculated production potential of NO_3+VOC at night during the spring campaign; **(b)** production potential ranking of VOCs at night during the spring campaign.

Table 3. Average concentrations, reaction branching, and SOA production of α-pinene, limonene, styrene, camphene, β-pinene, and isoprene with respect to different oxidants at night in the spring campaign.

Species	Concentration (ppbv)	Rate coefficient[a]		Branching ratio		SOA yield from the literature (with NO_3)	SOA from VOCs+NO_3 ($\mu g\,m^{-3}$)
		NO_3	O_3	NO_3	O_3		
α-Pinene	0.39	6.64E-12	7.2E-17	0.962	0.038	0–0.16[b]	0–0.33
Limonene	0.14	1.22E-11	1.54E-16	0.957	0.043	0.12–1.74[c]	0.09–1.28
Styrene	0.19	1.50E-12	1.70E-17	0.941	0.059	0.23[d]	0.24
Camphene	0.28	6.20E-13	9.0E-19	0.992	0.008	–	–
β-Pinene	0.01	2.51E-12	1.50E-17	0.968	0.032	0.07–1.04[e]	0.004–0.06
Isoprene	0.032	6.96E-13	1.27E-17	0.908	0.091	0.02–0.24[f]	0.002–0.02

[a] Rate coefficients for all species except camphene are from the Master Chemical Mechanism model (http://mcm.leeds.ac.uk/MCM/ (last access: 10 March 2019); under 25 °C), and rate coefficients for camphene are from Martínez et al. (1999) and Atkinson et al. (1990). [b] Hallquist et al. (1999), Spittler et al. (2006), Perraud et al. (2010), and Fry et al. (2014). [c] Fry et al. (2011, 2014), Spittler et al. (2006), and Boyd et al. (2017). [d] Cabrera-Perez et al. (2017). [e] Griffin et al. (1999), Fry et al. (2009, 2014), and Boyd et al. (2015). [f] Rollins et al. (2009) and Ng et al. (2008).

concentrations. On the other hand, although the BVOCs concentrations in Bakersfield were far less than those in other campaigns, the concentration of particulate organic nitrates there showed an intermediate level among all the campaigns. Therefore, it is suggested that the formation of particulate organic nitrates may be more relevant to NO_x than BVOCs, which is consistent with the finding that the organic nitrate production was dominated by NO_x in the southeastern US (Edwards et al., 2017). In the spring campaign of this study, we examined the correlation between organic nitrates and NO_2 or VOCs (by the sum of α pinene, limonene, camphene, and styrene) at night (Fig. S16) and found a significant correlation of organic nitrates with NO_2 ($R = 0.40$–0.47) rather than with VOCs ($R = 0.22$–0.23), which further suggests that the organic nitrate formation was driven by the NO_x-involved NO_3 chemistry.

4 Conclusions

An aerodyne HR-ToF-AMS was deployed in urban Shenzhen for about 1 month per season during 2015–2016 to characterize particulate organic nitrates with a high time resolution. We discovered high mass fractions of organic nitrates in total organics during warmer seasons, including spring (9 %–21 %), summer (11 %–25 %), and autumn (9 %–20 %), while particulate organic nitrates were negligible in winter. The correlation analysis between organic nitrates and each OA factor showed high correlation ($R = 0.77$ in spring, 0.91 in summer, and 0.72 in autumn) between organic nitrates and LO-OOA at night. The diurnal trend analysis of size distribution of the m/z 30 / m/z 46 ratio further suggested that organic nitrate formation mainly occurred at night. It also suggested that organic nitrates concentrated at smaller sizes, indicating that they were mostly local products. The calculated theoretical nighttime production potential of NO_3 reacting with VOCs measured in spring showed that six VOC species

Table 4. Average ambient temperatures, average concentrations of monoterpenes, $NO_{3,total}$, $NO_{3,org}$, $NO_{3,org}/NO_{3,total}$, and the ratio of organic nitrates to total organics (ON / Org) for different field campaigns around the world. The ON results at the European and US sites are from Kiendler-Scharr et al. (2016) and Ng et al. (2017).

Sampling site	Site type	Sampling period	Temperature (°C)	NO (ppbv)	NO_2 (ppbv)	Monoterpenes (ppbv)	$NO_{3,org}$ ($\mu g\ m^{-3}$)	$NO_{3,org}/NO_{3,total}$	ON / Org	Reference, note
Bakersfield, US	Rural	May–June 2010	23.0		8.2	0.045 (α-pinene) 0.004 (β-pinene) 0.034 (limonene)	0.16	0.28	0.23	Rollins et al. (2012), $NO_{3,org}$ measured by TD-LIF
Woodland Park, US	High attitude	July–August 2011	15.0		1.2	0.25 (monoterpene)	0.06	0.86	0.09	Fry et al. (2013), use AMS data to estimate $NO_{3,org}$
Centreville, US	Rural	June–July 2013	24.7	0.1	1.1	0.350 (α-pinene)* 0.312 (β-pinene)* 0.050 (limonene)*	0.08	1.00	0.10	Xu et al. (2015a, b), use AMS data to estimate $NO_{3,org}$
Barcelona, Spain	Urban	March 2009	13.3	11.0	23.6	0.423 (monoterpene)	0.48	0.13	0.13	Mohr et al. (2012) Pandolfi et al. (2014), use AMS data to estimate $NO_{3,org}$
Shenzhen, China	Urban	April 2016	24.5	8.0	19.4	0.391 (α-pinene)* 0.013 (β-pinene)* 0.137 (limonene)*	0.16	0.17	0.11	This study, use AMS data to estimate $NO_{3,org}$

* BVOC concentration at night.

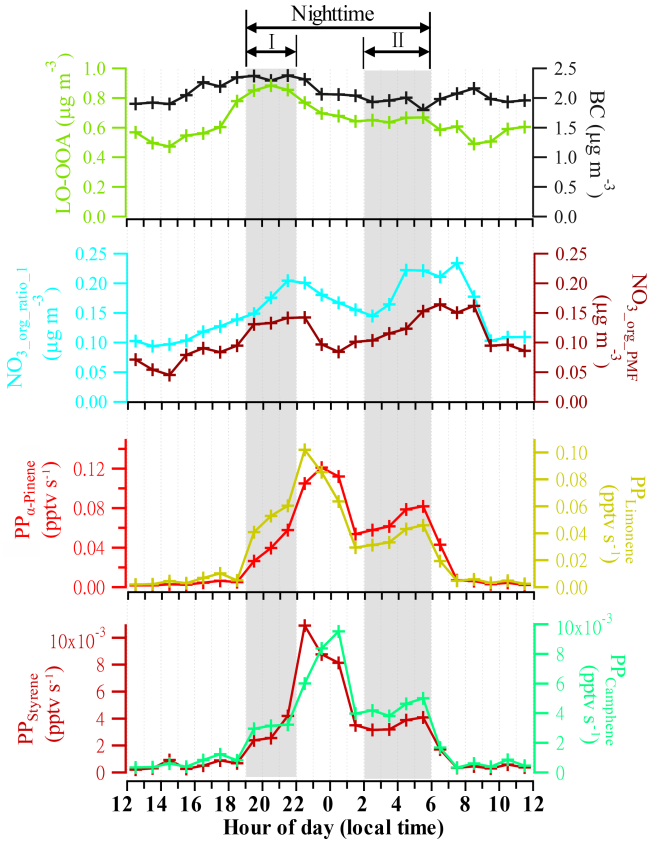

Figure 6. Diurnal trends of BC, LO-OOA, NO_{3,org_ratio_1}, and NO_{3,org_PMF}, and production potential (PP) of α-pinene, limonene, styrene, and camphene during the spring campaign.

(i.e., α-pinene, limonene, styrene, camphene, β-pinene, and isoprene) were prominent precursors. The SOA yield analysis and the nighttime variation in production potential further indicated that α-pinene, limonene, camphene, and styrene could contribute significantly to nighttime formation of particulate organic nitrates in spring in Shenzhen, highlighting the unique contribution of anthropogenic VOCs in comparison to that documented in previous studies in the US and Europe. Finally, the comparison of the results in this study with other similar studies implied that nighttime formation of particulate organic nitrates is more relevant to NO_x levels.

Data availability. The data in this study are available from the authors upon request (huangxf@pku.edu.cn).

Supplement. The supplement related to this article is available online at: https://doi.org/10.5194/acp-19-5235-2019-supplement.

Author contributions. XFH designed the research. KY and QZ conducted data analysis and wrote the paper. KD contributed to modeling and writing. KY and QZ contributed equally to this work.

Competing interests. The authors declare that they have no conflict of interest.

Acknowledgements. This work was supported by the National Key R&D Program of China (2018YFC0213901), National Natural Science Foundation of China (91544215; 41622304), and Science and Technology Plan of Shenzhen Municipality (JCYJ20170412150626172). The authors should like to thank the referees for helpful suggestions.

Review statement. This paper was edited by Nga Lee Ng and reviewed by three anonymous referees.

References

An, J. L., Wang, Y. S., and Sun, Y.: Effects of nonmethane hydrocarbons on ozone formation in Beijing, Ecology and Environmental Sciences, 18, 1318–1324, https://doi.org/10.16258/j.cnki.1674-5906.2009.04.03, 2009.

Atkinson, R., Aschmann, S. M., and Arey, J.: Rate constants for the gas-phase reactions of OH and NO_3 radicals and O_3 with sabinene and camphene at 296±2 K, Atmos. Environ., 24, 2647–2654, https://doi.org/10.1016/0960-1686(90)90144-C, 1990.

Ayres, B. R., Allen, H. M., Draper, D. C., Brown, S. S., Wild, R. J., Jimenez, J. L., Day, D. A., Campuzano-Jost, P., Hu, W., de Gouw, J., Koss, A., Cohen, R. C., Duffey, K. C., Romer, P., Baumann, K., Edgerton, E., Takahama, S., Thornton, J. A., Lee, B. H., Lopez-Hilfiker, F. D., Mohr, C., Wennberg, P. O., Nguyen, T. B., Teng, A., Goldstein, A. H., Olson, K., and Fry, J. L.: Organic nitrate aerosol formation via NO_3 + biogenic volatile organic compounds in the southeastern United States, Atmos. Chem. Phys., 15, 13377–13392, https://doi.org/10.5194/acp-15-13377-2015, 2015.

Boyd, C. M., Sanchez, J., Xu, L., Eugene, A. J., Nah, T., Tuet, W. Y., Guzman, M. I., and Ng, N. L.: Secondary organic aerosol formation from the β-pinene+NO_3 system: effect of humidity and peroxy radical fate, Atmos. Chem. Phys., 15, 7497–7522, https://doi.org/10.5194/acp-15-7497-2015, 2015.

Boyd, C. M., Nah, T., Xu, L., Berkemeier, T., and Ng, N. L.: Secondary Organic Aerosol (SOA) from Nitrate Radical Oxidation of Monoterpenes: Effects of Temperature, Dilution, and Humidity on Aerosol Formation, Mixing, and Evaporation, Environ. Sci. Technol., 51, 7831–7841. https://doi.org/10.1021/acs.est.7b01460, 2017.

Bruns, E. A., Perraud, V., Zelenyuk, A., Ezell, M. J., Johnson, S. N., Yu, Y., Imre, D., Finlayson-Pitts, B. J., and Alexander, M. L.: Comparison of FTIR and particle mass spectrometry for the measurement of particulate organic nitrates, Environ. Sci. Technol., 44, 1056–1061, https://doi.org/10.1021/es9029864, 2010.

Cabrera-Perez, D., Taraborrelli, D., Sander, R., and Pozzer, A.: Global atmospheric budget of simple monocyclic aromatic compounds, Atmos. Chem. Phys., 16, 6931–6947, https://doi.org/10.5194/acp-16-6931-2016, 2016.

Cabrera-Perez, D., Taraborrelli, D., Lelieveld, J., Hoffmann, T., and Pozzer, A.: Global impact of monocyclic aromatics on tropospheric composition, Atmos. Chem. Phys. Discuss., https://doi.org/10.5194/acp-2017-928, 2017.

Canagaratna, M. R., Jayne, J. T., Jimenez, J. L., Allan, J. D., Alfarra, M. R., Zhang, Q., Onasch, T. B., Drewnick, F., Coe, H., Middlebrook, A., Delia, A., Williams, L. R., Trimborn, A. M., Northway, M. J., DeCarlo, P. F., Kolb, C. E., Davidovits, P., and Worsnop, D. R.: Chemical and microphysical characterization of ambient aerosols with the aerodyne aerosol mass spectrometer, Mass Spectrom. Rev., 26, 185–222, https://doi.org/10.1002/mas.20115, 2007.

Cubison, M. J., Ortega, A. M., Hayes, P. L., Farmer, D. K., Day, D., Lechner, M. J., Brune, W. H., Apel, E., Diskin, G. S., Fisher, J. A., Fuelberg, H. E., Hecobian, A., Knapp, D. J., Mikoviny, T., Riemer, D., Sachse, G. W., Sessions, W., Weber, R. J., Weinheimer, A. J., Wisthaler, A., and Jimenez, J. L.: Effects of aging on organic aerosol from open biomass burning smoke in aircraft and laboratory studies, Atmos. Chem. Phys., 11, 12049–12064, https://doi.org/10.5194/acp-11-12049-2011, 2011.

DeCarlo, P. F., Kimmel, J. R., Trimborn, A., Northway, M. J., Jayne, J. T., Aiken, A. C., Gonin, M., Fuhrer, K., Horvath, T., Docherty, K. S., Worsnop, D. R., and Jimenez, J. L.: Field-deployable, high-resolution, time-of-flight aerosol mass spectrometer, Anal. Chem., 78, 8281–8289, https://doi.org/10.1021/ac061249n, 2006.

Edwards, P. M., Aikin, K. C., Dube, W. P., Fry, J. L., Gilman, J. B., de Gouw, J. A., Graus, M. G., Hanisco, T. F., Holloway, J., Hübler, G., Kaiser, J., Keutsch, F. N., Lerner, B. M., Neuman, J. A., Parrish, D. D., Peischl, J., Pollack, I. B., Ravishankara, A. R., Roberts, J. M., Ryerson, T. B., Trainer, M., Veres, P. R., Wolfe, G. M., Warneke, C., and Brown, S. S.: Transition from high- to low-NO_x control of night-time oxidation in the southeastern US, Nat. Geosci., 10, 490–495, https://doi.org/10.1038/ngeo2976, 2017.

Farmer, D. K., Matsunaga, A., Docherty, K. S., Surratt, J. D., Seinfeld, J. H., Ziemann, P. J., and Jimenez, J. L.: Response of an aerosol mass spectrometer to organonitrates and organosulfates and implications for atmospheric chemistry, P. Natl. Acad. Sci. USA, 107, 6670–6675, https://doi.org/10.1073/pnas.0912340107, 2010.

Fry, J. L., Kiendler-Scharr, A., Rollins, A. W., Wooldridge, P. J., Brown, S. S., Fuchs, H., Dubé, W., Mensah, A., dal Maso, M., Tillmann, R., Dorn, H.-P., Brauers, T., and Cohen, R. C.: Organic nitrate and secondary organic aerosol yield from NO_3 oxidation of β-pinene evaluated using a gas-phase kinetics/aerosol partitioning model, Atmos. Chem. Phys., 9, 1431–1449, https://doi.org/10.5194/acp-9-1431-2009, 2009.

Fry, J. L., Kiendler-Scharr, A., Rollins, A. W., Brauers, T., Brown, S. S., Dorn, H.-P., Dubé, W. P., Fuchs, H., Mensah, A., Rohrer, F., Tillmann, R., Wahner, A., Wooldridge, P. J., and Cohen, R. C.: SOA from limonene: role of NO_3 in its generation and degradation, Atmos. Chem. Phys., 11, 3879–3894, https://doi.org/10.5194/acp-11-3879-2011, 2011.

Fry, J. L., Draper, D. C., Zarzana, K. J., Campuzano-Jost, P., Day, D. A., Jimenez, J. L., Brown, S. S., Cohen, R. C., Kaser, L., Hansel, A., Cappellin, L., Karl, T., Hodzic Roux, A., Turnipseed, A., Cantrell, C., Lefer, B. L., and Grossberg,

N.: Observations of gas- and aerosol-phase organic nitrates at BEACHON-RoMBAS 2011, Atmos. Chem. Phys., 13, 8585–8605, https://doi.org/10.5194/acp-13-8585-2013, 2013.

Fry, J. L., Draper, D. C., Barsanti, K. C., Smith, J. N., Ortega, J., Winkler, P. M., Lawler, M. J., Brown, S. S., Edwards, P. M., and Cohen, R. C.: Secondary Organic Aerosol Formation and Organic Nitrate Yield from NO_3 Oxidation of Biogenic Hydrocarbons, Environ. Sci. Technol., 48, 11944–11953, https://doi.org/10.1021/es502204x, 2014.

Fry, J. L., Brown, S. S., Middlebrook, A. M., Edwards, P. M., Campuzano-Jost, P., Day, D. A., Jimenez, J. L., Allen, H. M., Ryerson, T. B., Pollack, I., Graus, M., Warneke, C., de Gouw, J. A., Brock, C. A., Gilman, J., Lerner, B. M., Dubé, W. P., Liao, J., and Welti, A.: Secondary organic aerosol (SOA) yields from NO_3 radical + isoprene based on nighttime aircraft power plant plume transects, Atmos. Chem. Phys., 18, 11663–11682, https://doi.org/10.5194/acp-18-11663-2018, 2018.

Griffin, R. J., Cocker III, D. R., Flagan, R. C., and Seinfeld, J. H.: Organic aerosol formation from the oxidation of biogenic hydrocarbons, J. Geophys. Res., 104, 3555–3567, https://doi.org/10.1029/1998jd100049, 1999.

Hallquist, M., Wängberg, I., Ljungström, E., Barnes, I., and Becker, K. H.: Aerosol and product yields from NO_3 radical-initiated oxidation of selected monoterpenes, Environ. Sci. Technol., 33, 553–559, https://doi.org/10.1021/es980292s, 1999.

Hao, L. Q., Kortelainen, A., Romakkaniemi, S., Portin, H., Jaatinen, A., Leskinen, A., Komppula, M., Miettinen, P., Sueper, D., Pajunoja, A., Smith, J. N., Lehtinen, K. E. J., Worsnop, D. R., Laaksonen, A., and Virtanen, A.: Atmospheric submicron aerosol composition and particulate organic nitrate formation in a boreal forestland–urban mixed region, Atmos. Chem. Phys., 14, 13483–13495, https://doi.org/10.5194/acp-14-13483-2014, 2014.

He, L. Y., Huang, X. F., Xue, L., Hu, M., Lin, Y., Zheng, J., Zhang, R., and Zhang, Y. H.: Submicron aerosol analysis and organic source apportionment in an urban atmosphere in Pearl River Delta of China using high-resolution aerosol mass spectrometry, J. Geophys. Res.-Atmos., 116, D12304, https://doi.org/10.1029/2010JD014566, 2011.

Huang, X.-F., He, L.-Y., Hu, M., Canagaratna, M. R., Sun, Y., Zhang, Q., Zhu, T., Xue, L., Zeng, L.-W., Liu, X.-G., Zhang, Y.-H., Jayne, J. T., Ng, N. L., and Worsnop, D. R.: Highly time-resolved chemical characterization of atmospheric submicron particles during 2008 Beijing Olympic Games using an Aerodyne High-Resolution Aerosol Mass Spectrometer, Atmos. Chem. Phys., 10, 8933–8945, https://doi.org/10.5194/acp-10-8933-2010, 2010.

Huang, X.-F., He, L.-Y., Xue, L., Sun, T.-L., Zeng, L.-W., Gong, Z.-H., Hu, M., and Zhu, T.: Highly time-resolved chemical characterization of atmospheric fine particles during 2010 Shanghai World Expo, Atmos. Chem. Phys., 12, 4897–4907, https://doi.org/10.5194/acp-12-4897-2012, 2012.

Huang, X. F., Xue, L., Tian, X. D., Shao, W. W., Sun, T., Gong, Z. H., Ju, W. W., Jiang, B., Hu, M., and He, L. Y.: Highly time-resolved carbonaceous aerosol characterization in Yangtze River Delta of China: Composition, mixing state and secondary formation, Atmos. Environ., 64, 200–207, https://doi.org/10.1016/j.atmosenv.2012.09.059, 2013.

Jimenez, J. L., Jayne, J. T., Shi, Q., Kolb, C. E., Worsnop, D. R., Yourshaw, I., Seinfeld, J. H., Flagan, R. C., Zhang, X. F., Smith, K. A., Morris, J. W., and Davidovits, P.: Ambient aerosol sampling using the aerodyne aerosol mass spectrometer, J. Geophys. Res.-Atmos., 108, 447–457, https://doi.org/10.1029/2001JD001213, 2003.

Kiendler-Scharr, A., Mensah, A. A., Friese, E., Topping, D., Nemitz, E., Prevot, A. S. H., Äijälä, M., Allan, J., Canonaco, F., Canagaratna, M., Carbone, S., Crippa, M., Dall Osto, M., Day, D. A., De Carlo, P., Di Marco, C. F., Elbern, H., Eriksson, A., Freney, E., Hao, L., Herrmann, H., Hildebrandt, L., Hillamo, R., Jimenez, J. L., Laaksonen, A., McFiggans, G., Mohr, C., O'Dowd, C., Otjes, R., Ovadnevaite, J., Pandis, S. N., Poulain, L., Schlag, P., Sellegri, K., Swietlicki, E., Tiitta, P., Vermeulen, A., Wahner, A., Worsnop, D., and Wu, H. C.: Organic nitrates from night-time chemistry are ubiquitous in the European submicron aerosol, Geophys. Res. Lett., 43, 7735–7744, https://doi.org/10.1002/2016GL069239, 2016.

Lee, B. H., Mohr, C., Lopez-Hilfiker, F. D., Lutz, A., Hallquist, M., Lee, L., Romer, P., Cohen, R. C., Iyer, S., Kurten, T., Hu, W., Day, D. A., Campuzano-Jost, P., Jimenez, J. L., Xu, L., Ng, N. L., Guo, H., Weber, R. J., Wild, R. J., Brown, S. S., Koss, A., de Gouw, J., Olson, K., Goldstein, A. H., Seco, R., Kim, S., McAvey, K., Shepson, P. B., Starn, T., Baumann, K., Edgerton, E. S., Liu, J., Shilling, J. E., Miller, D. O., Brune, W., Schobesberger, S., D'Ambro, E. L., and Thornton, J. A.: Highly functionalized organic nitrates in the southeast United States: Contribution to secondary organic aerosol and reactive nitrogen budgets, P. Natl. Acad. Sci. USA, 113, 1516–1521, https://doi.org/10.1073/pnas.1508108113, 2016.

Lelieveld, J., Gromov, S., Pozzer, A., and Taraborrelli, D.: Global tropospheric hydroxyl distribution, budget and reactivity, Atmos. Chem. Phys., 16, 12477–12493, https://doi.org/10.5194/acp-16-12477-2016, 2016.

Martínez, E., Cabañas, B., Aranda, A., Martín, P., and Salgado, S.: Absolute Rate Coefficients for the Gas-Phase Reactions of NO_3 Radical with a Series of Monoterpenes at T = 298 to 433 K, J. Atmos. Chem., 33, 265–282, https://doi.org/10.1023/A:1006178530211, 1999.

Matthew, B. M., Middlebrook, A. M., and Onasch, T. B.: Collection Efficiencies in an Aerodyne Aerosol Mass Spectrometer as a Function of Particle Phase for Laboratory Generated Aerosols, Aerosol Sci. Tech., 42, 884–898, https://doi.org/10.1080/02786820802356797, 2008.

Middlebrook, A. M., Bahreini, R., Jimenez, J. L., and Canagaratna, M. R.: Evaluation of composition-dependent collection efficiencies for the Aerodyne aerosol mass spectrometer using field data, Aerosol Sci. Tech., 46, 258–271, https://doi.org/10.1080/02786826.2011.620041, 2012.

Mohr, C., DeCarlo, P. F., Heringa, M. F., Chirico, R., Slowik, J. G., Richter, R., Reche, C., Alastuey, A., Querol, X., Seco, R., Peñuelas, J., Jiménez, J. L., Crippa, M., Zimmermann, R., Baltensperger, U., and Prévôt, A. S. H.: Identification and quantification of organic aerosol from cooking and other sources in Barcelona using aerosol mass spectrometer data, Atmos. Chem. Phys., 12, 1649–1665, https://doi.org/10.5194/acp-12-1649-2012, 2012.

Nah, T., Sanchez, J., Boyd, C. M., and Ng, N. L.: Photochemical Aging of α-pinene and β-pinene Secondary Organic Aerosol formed from Nitrate Radical Oxidation, Environ. Sci. Technol.,

50, 222–231, https://https://doi.org/10.1021/acs.est.5b04594, 2016.

Ng, N. L., Kwan, A. J., Surratt, J. D., Chan, A. W. H., Chhabra, P. S., Sorooshian, A., Pye, H. O. T., Crounse, J. D., Wennberg, P. O., Flagan, R. C., and Seinfeld, J. H.: Secondary organic aerosol (SOA) formation from reaction of isoprene with nitrate radicals (NO_3), Atmos. Chem. Phys., 8, 4117–4140, https://doi.org/10.5194/acp-8-4117-2008, 2008.

Ng, N. L., Canagaratna, M. R., Zhang, Q., Jimenez, J. L., Tian, J., Ulbrich, I. M., Kroll, J. H., Docherty, K. S., Chhabra, P. S., Bahreini, R., Murphy, S. M., Seinfeld, J. H., Hildebrandt, L., Donahue, N. M., DeCarlo, P. F., Lanz, V. A., Prévôt, A. S. H., Dinar, E., Rudich, Y., and Worsnop, D. R.: Organic aerosol components observed in Northern Hemispheric datasets from Aerosol Mass Spectrometry, Atmos. Chem. Phys., 10, 4625–4641, https://doi.org/10.5194/acp-10-4625-2010, 2010.

Ng, N. L., Brown, S. S., Archibald, A. T., Atlas, E., Cohen, R. C., Crowley, J. N., Day, D. A., Donahue, N. M., Fry, J. L., Fuchs, H., Griffin, R. J., Guzman, M. I., Herrmann, H., Hodzic, A., Iinuma, Y., Jimenez, J. L., Kiendler-Scharr, A., Lee, B. H., Luecken, D. J., Mao, J., McLaren, R., Mutzel, A., Osthoff, H. D., Ouyang, B., Picquet-Varrault, B., Platt, U., Pye, H. O. T., Rudich, Y., Schwantes, R. H., Shiraiwa, M., Stutz, J., Thornton, J. A., Tilgner, A., Williams, B. J., and Zaveri, R. A.: Nitrate radicals and biogenic volatile organic compounds: oxidation, mechanisms, and organic aerosol, Atmos. Chem. Phys., 17, 2103–2162, https://doi.org/10.5194/acp-17-2103-2017, 2017.

Pandolfi, M., Querol, X., Alastuey, A., Jimenez, J. L., Jorba, O., Day, D., Ortega, A., Cubison, M. J., Comerón, A., Sicard, M., Mohr, C., Prévôt, A. S. H., Minguillón, M. C., Pey, J., Baldasano, J. M., Burkhart, J. F., Seco, R., Peñuelas, J., van Drooge, B. L., Artiñano, B., Di Marco, C., Nemitz, E., Schallhart, S., Metzger, A., Hansel, A., Lorente, J., Ng, S., Jayne, J., and Szidat, S.: Effects of sources and meteorology on particulate matter in the Western Mediterranean Basin: An overview of the DAURE campaign, J. Geophys. Res.-Atmos., 119, 4978–5010, https://10.1002/2013JD021079, 2014.

Perraud, V., Bruns, E. A., Ezell, M. J., Johnson, S. N., Greaves, J., and Finlayson-Pitts, B. J.: Identification of organic nitrates in the NO_3 radical initiated oxidation of α-pinene by atmospheric pressure chemical ionization mass spectrometry, Environ. Sci. Technol., 44, 5887–5893, https://doi.org/10.1021/es1005658, 2010.

Rollins, A. W., Browne, E. C., Min, K.-E., Pusede, S. E., Wooldridge, P. J., Gentner, D. R., Goldstein, A. H., Liu, S., Day, D. A., Russell, L. M., and Cohen, R. C.: Evidence for NO_x Control over Nighttime SOA Formation, Science, 337, 1210–1212, https://doi.org/10.1126/science.1221520, 2012.

Rollins, A. W., Kiendler-Scharr, A., Fry, J. L., Brauers, T., Brown, S. S., Dorn, H.-P., Dubé, W. P., Fuchs, H., Mensah, A., Mentel, T. F., Rohrer, F., Tillmann, R., Wegener, R., Wooldridge, P. J., and Cohen, R. C.: Isoprene oxidation by nitrate radical: alkyl nitrate and secondary organic aerosol yields, Atmos. Chem. Phys., 9, 6685–6703, https://doi.org/10.5194/acp-9-6685-2009, 2009.

Sato, K., Takami, A., Isozaki, T., Hikida, T., Shimono, A., and Imamura, T.: Mass spectrometric study of secondary organic aerosol formed from the photo-oxidation of aromatic hydrocarbons, Atmos. Environ., 44, 1080–1087, https://doi.org/10.1016/j.atmosenv.2009.12.013, 2010.

Sobanski, N., Thieser, J., Schuladen, J., Sauvage, C., Song, W., Williams, J., Lelieveld, J., and Crowley, J. N.: Day and nighttime formation of organic nitrates at a forested mountain site in south-west Germany, Atmos. Chem. Phys., 17, 4115–4130, https://doi.org/10.5194/acp-17-4115-2017, 2017.

Spittler, M., Barnes, I., Bejan, I., Brockmann, K. J., Benter, T., and Wirtz, K.: Reactions of NO_3 radicals with limonene and α-pinene: Product and SOA formation, Atmos. Environ., 40, 116–127, https://doi.org/10.1016/j.atmosenv.2005.09.093, 2006.

Sun, Y. L., Zhang, Q., Schwab, J. J., Yang, T., Ng, N. L., and Demerjian, K. L.: Factor analysis of combined organic and inorganic aerosol mass spectra from high resolution aerosol mass spectrometer measurements, Atmos. Chem. Phys., 12, 8537–8551, https://doi.org/10.5194/acp-12-8537-2012, 2012.

Teng, A. P., Crounse, J. D., Lee, L., St. Clair, J. M., Cohen, R. C., and Wennberg, P. O.: Hydroxy nitrate production in the OH-initiated oxidation of alkenes, Atmos. Chem. Phys., 15, 4297–4316, https://doi.org/10.5194/acp-15-4297-2015, 2015.

Teng, A. P., Crounse, J. D., and Wennberg, P. O.: Isoprene Peroxy Radical Dynamics, J. Am. Chem. Soc., 15, 4297–4316, https://doi.org/10.1021/jacs.6b12838, 2017.

Wang, M., Zeng, L., Lu, S., Shao, M., Liu, X., Yu, X., Chen, W., Yuan, B., Zhang, Q., Hu, M., and Zhang, Z.: Development and validation of a cryogen-free automatic gas chromatograph system (GC-MS/FID) for online measurements of volatile organic compounds, Anal. Methods-UK, 6, 9424–9434, https://doi.10.1039/C4AY01855A, 2014.

Xu, L., Guo, H., Boyd, C. M., Klein, M., Bougiatioti, A., Cerully, K. M., Hite, J. R., Isaacman-VanWertz, G., Kreisberg, N. M., Knote, C., Olson, K., Koss, A., Goldstein, A. H., Hering, S. V., de Gouw, J., Baumann, K., Lee, S.-H., Nenes, A., Weber, R. J., and Ng, N. L.: Effects of anthropogenic emissions on aerosol formation from isoprene and monoterpenes in the southeastern United States, P. Natl. Acad. Sci. USA, 112, 37–42, https://doi.org/10.1073/pnas.1417609112, 2015a.

Xu, L., Suresh, S., Guo, H., Weber, R. J., and Ng, N. L.: Aerosol characterization over the southeastern United States using high-resolution aerosol mass spectrometry: spatial and seasonal variation of aerosol composition and sources with a focus on organic nitrates, Atmos. Chem. Phys., 15, 7307–7336, https://doi.org/10.5194/acp-15-7307-2015, 2015b.

Xu, W., Sun, Y., Wang, Q., Du, W., Zhao, J., Ge, X., Han, T., Zhang, Y., Zhou, W., Li, J., Fu, P., Wang, Z., and Worsnop, D. R.: Seasonal Characterization of Organic Nitrogen in Atmospheric Aerosols Using High Resolution Aerosol Mass Spectrometry in Beijing, China, ACS Earth Sp. Chem., 1, 673–682, https://doi.org/10.1021/acsearthspacechem.7b00106, 2017.

Yuan, B., Hu, W. W., Shao, M., Wang, M., Chen, W. T., Lu, S. H., Zeng, L. M., and Hu, M.: VOC emissions, evolutions and contributions to SOA formation at a receptor site in eastern China, Atmos. Chem. Phys., 13, 8815–8832, https://doi.org/10.5194/acp-13-8815-2013, 2013.

Zhang, Q., Jimenez, J. L., Canagaratna, M. R., Ulbrich, I. M., Ng, N. L., Worsnop, D. R., and Sun, Y.: Understanding atmospheric organic aerosols via factor analysis of aerosol mass spectrometry: A revie, Anal. Bioanal. Chem., 401, 3045–3067, https://doi.org/10.1007/s00216-011-5355-y, 2011.

Zhang, Y. H., Su, H., Zhong, L. J., Cheng, Y. F., Zeng, L. M., Wang, X. S., Xiang, Y. R., Wang, J. L., Gao, D. F., Shao, M., Fan, S. J.,

and Liu, S. C.: Regional ozone pollution and observation-based approach for analyzing ozone-precursor relationship during the PRIDE-PRD2004 campaign, Atmos. Environ., 42, 6203–6218, https://doi.org/10.1016/j.atmosenv.2008.05.002, 2008.

Zhu, B., Han, Y., Wang, C., Huang, X. F., Xia, S. Y., Niu, Y. B., Yin, Z. X., and He, L. Y.: Understanding primary and secondary sources of ambient oxygenated volatile organic compounds in Shenzhen utilizing photochemical age-based parameterization method, J. Environ. Sci., 75, 105–114, https://doi.org/10.1016/j.jes.2018.03.008, 2019.

Zhu, Q., He, L.-Y., Huang, X.-F., Cao, L.-M., Gong, Z.-H., Wang, C., Zhuang, X., and Hu, M.: Atmospheric aerosol compositions and sources at two national background sites in northern and southern China, Atmos. Chem. Phys., 16, 10283–10297, https://doi.org/10.5194/acp-16-10283-2016, 2016.

Zhu, Q., Huang, X.-F., Cao, L.-M., Wei, L.-T., Zhang, B., He, L.-Y., Elser, M., Canonaco, F., Slowik, J. G., Bozzetti, C., El-Haddad, I., and Prévôt, A. S. H.: Improved source apportionment of organic aerosols in complex urban air pollution using the multilinear engine (ME-2), Atmos. Meas. Tech., 11, 1049–1060, https://doi.org/10.5194/amt-11-1049-2018, 2018.